Chimera Simulations of Multibladed Rotors in High-Speed Forward Flight with Weak Fluid-Structure-Coupling

Klausdieter Pahlke
DLR, Institute of Aerodynamics and Fluid Technology
D-38108 Braunschweig, Lilienthalplatz 7
email: Klausdieter.Pahlke@dlr.de

Berend G. van der Wall
DLR, Institute of Flight Research
D-38108 Braunschweig, Lilienthalplatz 7
email: Berend.vanderWall@dlr.de

Abstract: The state of the art of weak fluid-structure coupling for rotors in forward flight at DLR is presented. The coupling procedure is based on the DLR rotor simulation code S4 and the DLR Navier-Stokes solver for structured grids FLOWer. The method allows to produce trimmed CFD solutions for rotors in high-speed forward flight with inclusion of elastic blade deformations and viscous effects. The weak coupling procedure is applied to high-speed forward flight test cases of the 7A and the 7AD rotor. The full 4-bladed rotor is simulated for both cases using the chimera approach. A variation of turbulence models from algebraic to 2 equation models did not show significant differences for these high-speed forward flight test cases with moderate rotor loading. The weak coupling which includes the transfer of normal forces (c_n), tangential forces (c_t) and pitching moments (c_m) from the CFD code to the rotor simulation code improved the overall agreement with the existing experimental data compared to the uncoupled computations considerably. The performance difference between the 7A and the 7AD rotor in high-speed forward flight is well predicted.

Nomenclature:

a_∞	free stream speed of sound
b	number of blades
c	local blade chord
c_mM^2	local pitching moment coefficient ($P/(0.5\rho_\infty a_\infty^2 c^2$ unit length))
c_nM^2	local normal force coefficient ($N/(0.5\rho_\infty a_\infty^2 c$ unit length))
c_tM^2	tangential force coefficient ($T/(0.5\rho_\infty a_\infty^2 c$ unit length))
k	specific kinetic turbulence energy
M	local reference Mach number
M_∞	free stream Mach number
$M_{\omega R}$	Mach number due to rotational motion of the blade tip ($\omega R/a_\infty$)
N	normal force [N]
P	pitching moment [Nm]
r	radial coordinate [m]
R	rotor radius [m]
T	tangential force [N]
Xb	non-dimensional propulsive force (see definition of Zb)
y+	non-dimensional distance normal to the blade surface
Zb	non-dimensional lift force $=100*\text{liftforce}/(0.5\rho_\infty * b * c_{root} * R * (\omega R)^2)$
α_q	rotor shaft angle [°]
β	flapping angle [°] at blade hinge $\beta=\beta_0+\beta_S\sin(\psi)+\beta_C\cos(\psi)+.....$
μ	advance ratio ($M_\infty/ M_{\omega R}$)
ϑ	elastic torsion angle [°]
θ	pitch angle [°], $\theta=\theta_0+\theta_S\sin(\psi)+\theta_C\cos(\psi)$
θ_0	collective pitch angle [°]
θ_C	lateral pitch angle [°]
θ_S	longitudinal pitch angle [°]
ψ	azimuth angle [°]
ω	rotational angular velocity [rad/s] or dissipation rate in 2-equation turbulence model

Introduction

One of the main tasks of CFD is to help in selecting the best shape of a body with respect to certain requirements. In the case of a helicopter rotor such requirements may be the best aerodynamic performance in forward flight or in hover, the best ride comfort, the lowest noise emission, etc. This paper deals with the application of RANS-methods for the prediction of aerodynamic performance of rotors in high-speed forward flight.

The comparison of two rotors requires identical flight conditions (i.e. the same lift and propulsive force, same global pitching and rolling moments). Hence a trim procedure for the CFD method is mandatory. The correct prediction of rotor blade aerodynamics for realistic rotors requires furthermore a simulation with elastic blades including fluid-structure coupling. This requires the inclusion of viscous effects (see [3])

in order to compute proper local pitching moments.
The above mentioned requirements can be met for constant level flight with weak and strong fluid-structure coupling approaches [4]. Since weak coupling is computational considerably less expensive than strong coupling the weak coupling approach was chosen for this paper. Several flavours of weak coupling have been published in the literature, ranging from a coupling that passes only normal forces [1], c_n, from the CFD method to the rotor simulation code (which means that the inherent 2D aerodynamics of the rotor simulation code is used for tangential forces and pitching moments) to a coupling that exchanges normal, tangential forces, c_t, *and* the pitching moment, c_m. As explained in [2] and [19] only the exchange of c_n, c_t and c_m provides a trim and blade motion which is independent of the simplified aerodynamic model of the underlying rotor simulation code.
All results within this paper were obtained by considering all degrees of freedom of a rotor blade (i.e. flap, lead-lag, pitching motion, elastic motions) with a weak coupling that includes normal forces, tangential forces *and* pitching moments.
A survey of selected literature on fluid-structure coupling with CFD methods until the year 2002 is given in [19]. A very interesting investigation was published in 2003 in [5], [6] where it was attempted to isolate the aerodynamics and structural dynamics for rotors in high-speed forward flight.

Solution Algorithm

CFD Solver FLOWer

All computations of this paper have been computed with a modified version of the block-structured DLR flow solver FLOWer [7] (Release 116.6). FLOWer is a portable software system and can be run on a large variety of computers with high efficiency. It solves the unsteady Reynolds-averaged Navier-Stokes equations, transformed into a moving blade fixed coordinate system. Details of the algorithm are given in [8]. The discretisation of space and time is separated following the method of lines [9] using a cell-vertex finite volume formulation for the spatial discretisation. In order to avoid spurious oscillations, a blend of first and third order dissipative terms is introduced. Two layers of auxiliary points are used to store the neighbour flow values in order to match the solutions across inner and external cuts with second order accuracy. In the code, different turbulence models are available. In the present work the algebraic Baldwin-Lomax model [10] with the modification of Degani and Schiff [11] and two versions of the 2-equation k-ω model (k-ω Wilcox [12], k-ω LEA [13] with Kok-modification for vortices [14]) are applied (see chapter 'Results' for further details). The time integration uses the dual time stepping technique with a second order implicit time integration operator [15]. An important speed-up of the computations is achieved by the multigrid technique. In order to allow for elastic blade motions deforming grids are used. Free stream consistency for deforming grids is guaranteed by a geometrical conservation law [16]. At each time step the deformed blade surface is computed using a Fourier series for each of the blade mode shapes which was calculated with the rotor simulation code S4. The deformed volume grid is then generated using transfinite interpolation techniques.

Rotor Simulation Code S4

The DLR rotor simulation code S4 originally was developed to compute effects of Higher Harmonic Control (HHC) onto dynamic rotor forces of a hingeless rotor in the non-rotating frame [17], [18]. With time, it evolved into a comprehensive code for the computation of isolated rotors with high resolution blade loads for acoustic post processing. It is validated by studies about active control of HHC or Individual Blade Control (IBC) [20], and the effects of dynamic stall [21]. It mainly consists of 3 modules:
The aerodynamics, the structural dynamics and the induced velocities module. An overview with some more details about S4 is given in [19].
The overall handling is done with an automatic trim module for specified non-rotating hub forces and moments. As degrees of freedom to trim to the desired values, the collective and cyclic controls are used; and in addition the rotor shaft angle of attack is taken. The rotor trim is defined by measured values of vertical and propulsive forces, plus pitch and roll moment, and the wind tunnel data like temperature, pressure, and velocity.

Coupling Procedure for Weak Coupling

The coupling between the CFD method FLOWer and the rotor simulation code S4 is carried out as follows (see Figure 1). First a trim computation is carried out with S4 alone using the simplified S4 aerodynamics. After this trim computation the elastic blade motion based on the aerodynamic forces of the blade element theory is known. The CFD code is then applied with this blade motion as prescribed boundary condition and provides a field of aerodynamic forces and moments for each blade element and each azimuth position.

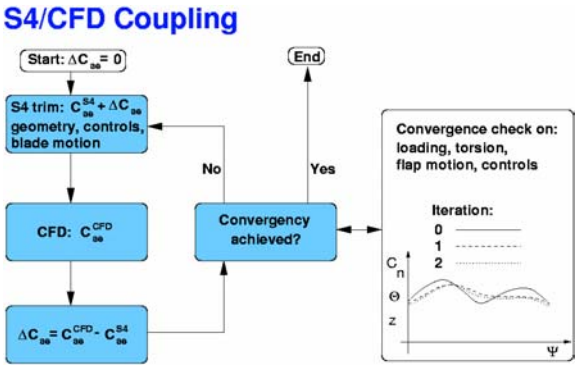

Figure 1 Block diagram of coupling procedure

The difference between the CFD aerodynamics and the S4 aerodynamics is computed. This difference is added to the S4 aerodynamic model in terms of normal forces (c_nM^2), tangential forces (c_tM^2) *and* pitching moments (c_mM^2) for the next iteration (see Figure 1). The new trim is now obtained based on the S4 aerodynamics plus the difference to the CFD aerodynamics. No relaxation for this difference is done. The full difference is applied. This procedure is repeated until the blade motion (control angles, rotor shaft angle and elastic blade motion) between two consecutive iterations is below a certain threshold.

By this coupling method the equation of motion of the rotor blade is solved with the aerodynamic forces and moments computed by the CFD method if the iteration process converges. In isolated blade computations the blade wake can only be computed inside the CFD grid. When complete rotors are computed (even with the chimera method), the individual vortices are diffused due to numerical dissipation as a consequence of the coarseness of the CFD grids some chords away from the blade. This problem is associated with a loss of blade-vortex interaction (BVI) effects, and is overcome by the following procedure: The CFD results contain harmonics usually up to 10/rev, with rather small amplitudes in the frequencies above 10/rev. Therefore the CFD results are low-pass filtered at 10/rev, and the same is done with the S4 loads, which do include BVI due to the prescribed wake used. An aerodynamic difference matrix is computed for this low frequency content (e.g. $\Delta c_nM^2 = c_nM^2(CFD) - c_nM^2(S4)$) and added to the next S4 trim as a non-variable aerodynamic offset. Thus, after convergence is obtained, the first 10 harmonics represent exactly the CFD aerodynamics, and all higher harmonics include BVI effects from S4, which are not contained in the CFD results. In the two test cases to be presented in this paper no strong BVI occurs. Therefore no differences were noticed compared to the procedure described above when all harmonics were taken from the CFD simulation and no harmonics from S4.

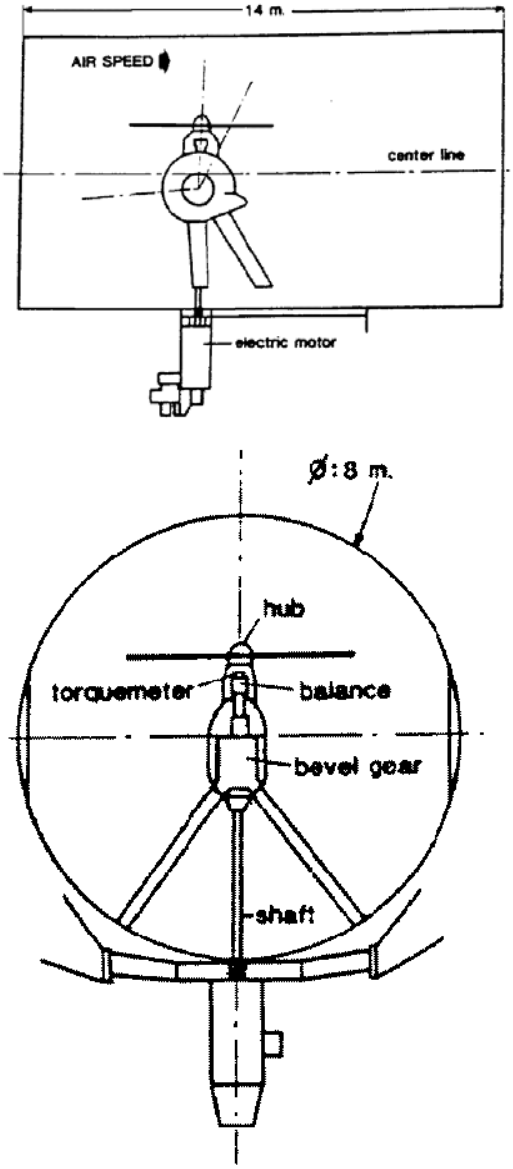

Figure 2 Experimental setup of the rotor test rig in the S1MA wind tunnel (top: side view, bottom: front view) [22]

Test Cases

High-speed forward flight test cases of the fully articulated 4-bladed ONERA 7A and 7AD rotors were selected. The 7A and the 7AD rotors are fully instrumented rotors which were designed by ECF and tested in the ONERA S1 wind tunnel at the Modane test center (see [23]). Figure 2 presents a sketch of the test setup including some geometric details of the model support and the rotor hub. The diameter of the wind tunnel test section is 8 m while the rotor diameter is 4.2 m. The 7A rotor has rectangular

blades whereas the 7AD rotor has a parabolic swept back tip with anhedral and a straight trailing edge. Both rotors have an aspect ratio of R/c_{root}=15. The test cases chosen correspond to a rotational tip speed Mach number of $M_{\omega R}$=0.64 with an advance ratio of μ=0.4, a lift coefficient of Zb=12.56 and a propulsive force coefficient of Xb=1.6. Chordwise pressure distributions were measured at 5 spanwise stations (0.5R, 0.7R, 0.825R, 0.915R, 0.975R). The integration of these pressures is used to compute the experimental normal force coefficients and pitching moments at these stations.

Grid Generation

Details about the grid generation can be found in [19]. This chapter repeats only the main features of the chimera grid system. In order to simplify the grid generation it was decided not to grid the whole test rig including the wind tunnel walls but to restrict oneself to an isolated 4-bladed rotor in perfect free flight conditions. Furthermore neither the rotor head nor the hub fairing were descretised. Hence only the four blades of the rotor are considered within the CFD simulations. The grid system consists of 4 child grids (CH type, one child grid for each blade) and a Cartesian background grid. A view of the whole grid system for the 7A rotor is presented in Figure 3.
A section of one child grid at r/R=0.9 is shown in Figure 4. In Figure 5 the grid in the rotor plane of the 7AD rotor is plotted. Please note the parabolic swept back tip of the 7AD rotor.

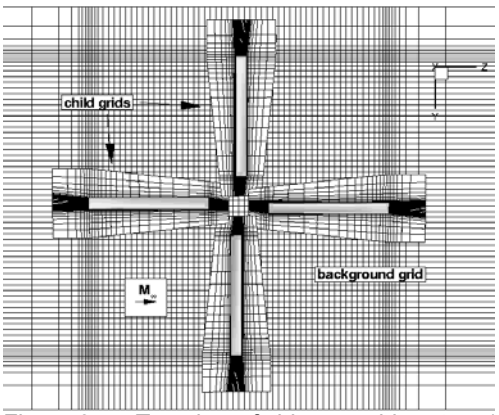

Figure 3 Top view of chimera grid system (7A)

The child grids for the chimera grid system around the 7A rotor were generated such that the distance from the blade surface to the outer boundary of the child grids is about 3c. The far field distance (i.e. the distance of the blade surface to the outer boundary of the background grid) is at minimum 1R in all directions. A Cartesian background grid with non-equidistant spacing was used (see Figure 3, only every other grid point printed).

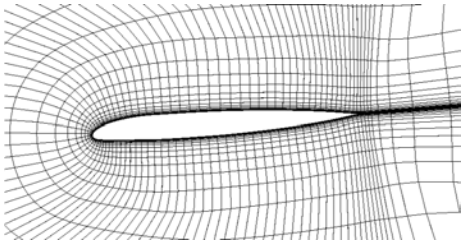
Figure 4 Grid section at r/R=0.9

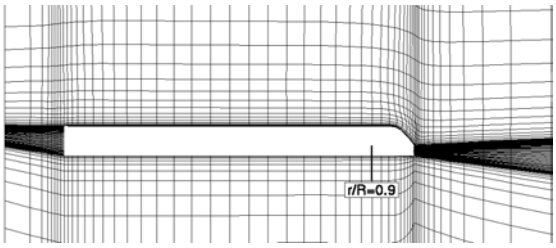

Figure 5 Grid in rotor plane for the 7AD rotor

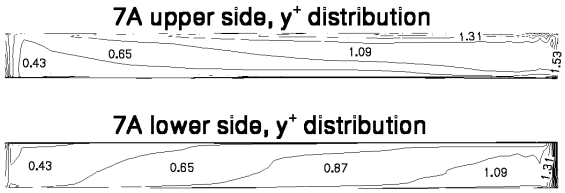

Figure 6 y+-distribution on the blade surface (7A rotor)

Figure 6 shows the y^+-distribution of the first grid points normal to the wall for the 7A rotor at $\psi=0^o$. The first grid spacing was set to 1.5e-5 c_{root} which corresponds to y^+-values of about 1 for a Reynolds number of about 2e+6. The most part of the blade has y^+-values which are around 1. At the very leading edge on the upper side y^+-values up to 2.5 are reached between r/R=0.7 and r/R=1.0. Only in the last row of cells at the very tip the y^+-values are between 2.5 and 3.5. This distribution of y^+-values is acceptable for resolving the high velocity gradients close to the blade surface. Still it should be kept in mind that this grid has only about 20 cells in the boundary layer which reproduces the main viscous effects but which cannot give a fully grid converged flow solution in the boundary layer. The flow was assumed to be fully turbulent.
The grid dimensions are:

Table 1: Number of grid cells

				Cells on blade surface		
	I	J	K	I	K	Total
isol. bl.	128	40	56	96	32	286 720
Chimera Child (per blade)	144	48	68	96	48	470 016
Chimera Back-ground	64	144	144			1.3 e6
Chimera total						3.2 e6

The I-direction corresponds to the wrap-around direction, the J-direction to the direction normal to the blade surface and the K-direction to the radial direction. The blade descretisation for the S4 code consists of 20 blade elements with a reduced element size close to the blade tip. Further details on the blade discretisation are given in Figure 7 for S4 and Table 1 for CFD.

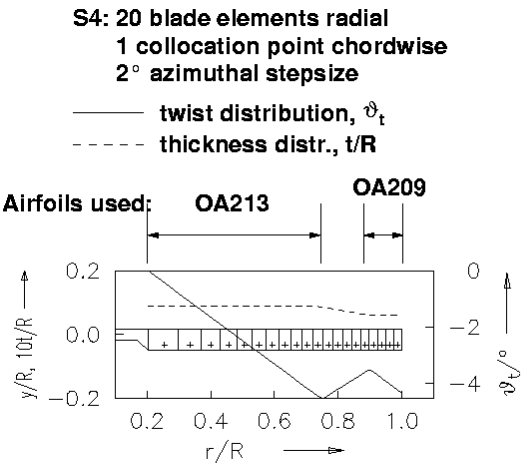

Figure 7 Blade discretisation for S4

Results

Selection of Turbulence model

A prerequisite for any solution of the Reynolds averaged Navier-Stokes equations is an appropriate turbulence model. This chapter concerns itself with an investigation of the effect of different turbulence models on the aerodynamic prediction of the above mentioned rotor test cases. In order to be as close as possible to the real test case but to reduce at the same time the computational costs considerably the following features were selected for this investigation:

Only isolated blade computations with elastic blades and the same prescribed realistic blade motion for all turbulence models are carried out. This means that only the effect of the turbulence model in the near-field of the blade will be assessed, different vortex conservation properties will not be considered. All computations will be done for fully turbulent flow. The differences between the turbulence models will be checked in terms of c_n, c_t, c_m and surface streamlines. This paper is focussed on dominant aerodynamic features which directly effect the rotor trim. Therefore no detailed comparisons of velocity profiles in the boundary layer are done.
The following models will be compared:
As a reference the standard Baldwin-Lomax model [10] with Degani-Schiff modification [11] for reduced viscosity in vortices was chosen. The second model is the widely used standard 2-equation k-ω model from Wilcox [12]. This model is well suited for moderate flow separation, it is independent of wall distance and therefore well suited to general MB grid systems. A well known disadvantage of this model is the too high level of viscosity in vortices. The third model is the k-ω LEA turbulence model [13] with Kok- modification for vortices [14]. This model has similar basic features as the k-ω Wilcox model but represents in addition the linear part of a non-linear explicit algebraic stress model. It is therefore assumed to be more accurate, especially for cases with flow separation. In order to reduce the viscosity in vortices a specific modification as proposed by Kok was implemented.
Figure 8 - Figure 10 present the streamlines on the upper side of the blades for the 7A rotor test case for four azimuth positions, i.e. 0^o, 90^o, 180^o and 270^o. Although we can detect several regions with flow separation all models compute very similar flow patterns. This is confirmed by a comparison of the normal forces in Figure 11, the tangential forces in Figure 12 and the pitching moments in Figure 13.
It can be concluded that for this specific test case of a rotor with moderate loading in high-speed forward flight no significant improvements are obtained by using more sophisticated turbulence models than the Baldwin-Lomax model. Therefore no further tests with other even more sophisticated turbulence models were carried out for this configuration. All computations in the following chapters apply the Baldwin-Lomax model with the Degani-Schiff modification because its CPU time consumption is about 50% lower than for the 2-equation k-ω type models.

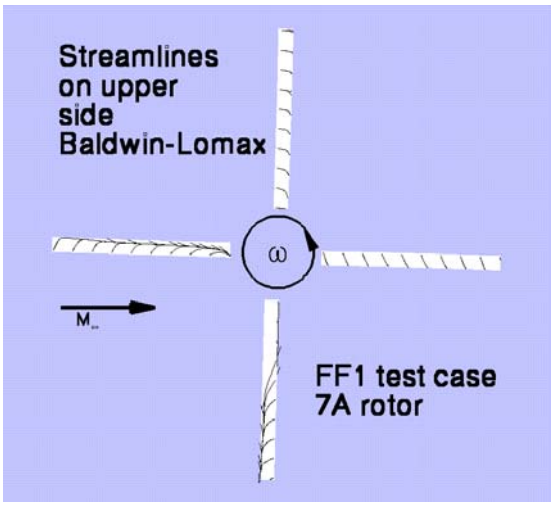

Figure 8 Streamlines on the upper side of the blades for the Baldwin-Lomax turbulence model (7A rotor)

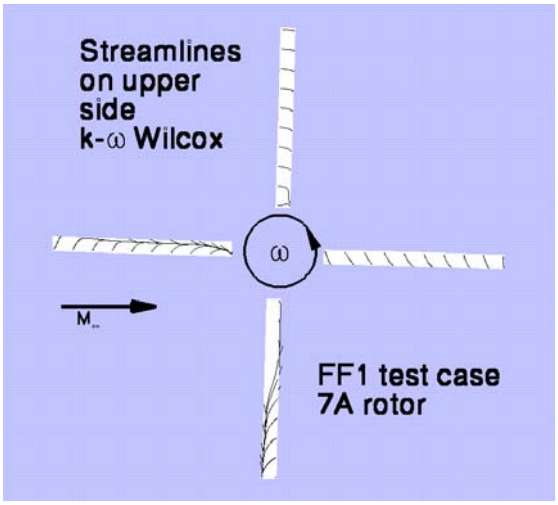

Figure 9 Streamlines on the upper side of the blades for the standard k-ω turbulence model (7A rotor)

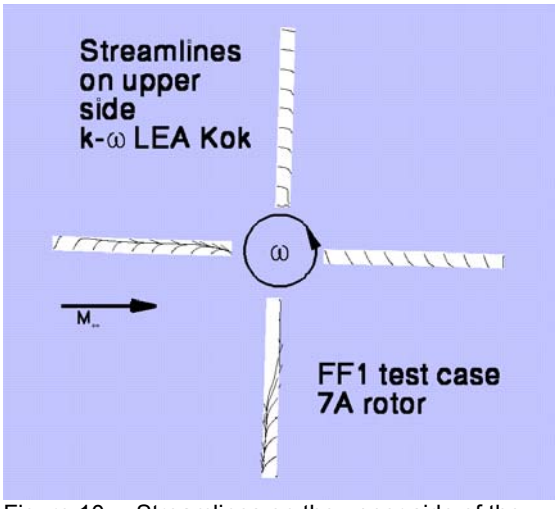

Figure 10 Streamlines on the upper side of the blades for the k-ω LEA turbulence model with Kok modification (7A rotor)

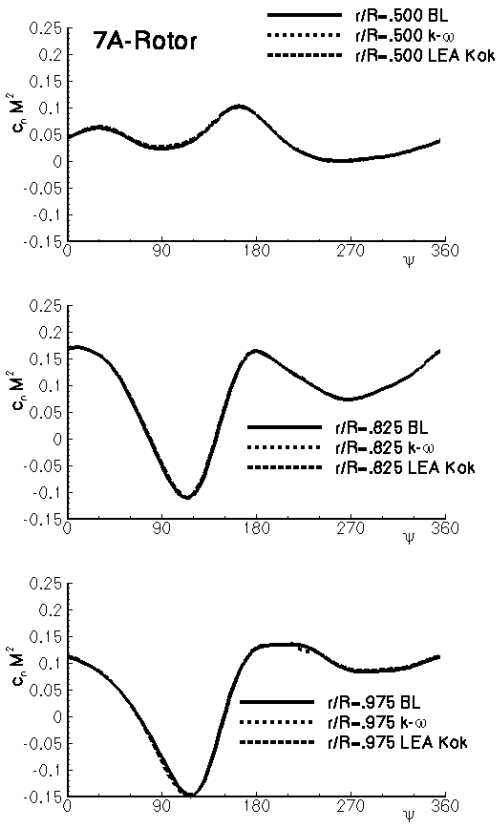

Figure 11 Normal force distributions of isol. bl. comp. with 3 turb. models (7A rotor)

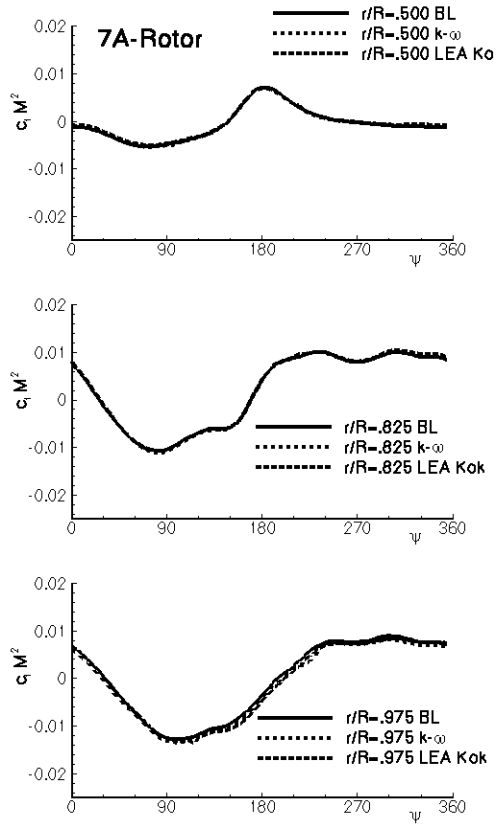

Figure 12 Tangential force distributions of the isolated blade computations with 3 turbulence models (7A rotor)

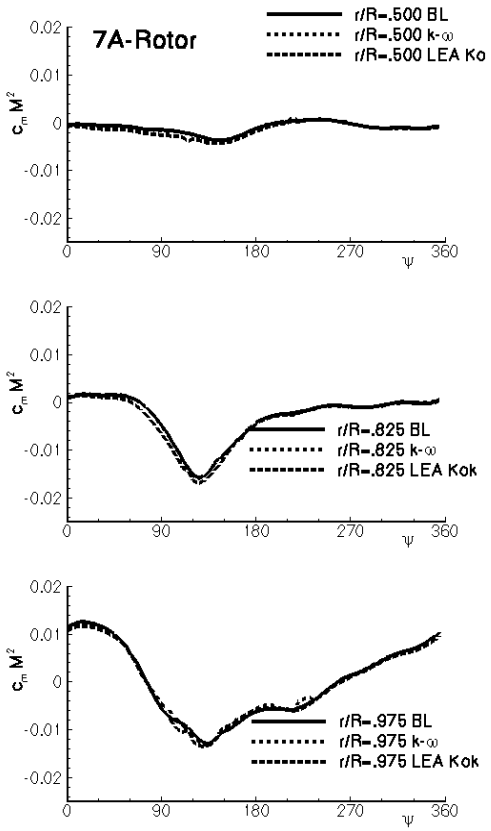

Figure 13 Moment distributions of the isolated blade computations with 3 turbulence models (7A rotor)

Multi-bladed Computation for the 7A Rotor with c_n+c_t+c_m-Coupling

All following results in this paper have been obtained for the 4-bladed rotor with a weak coupling that includes normal forces, tangential forces and pitching moments. The chimera technique is applied in order to capture the wake system and to allow for the relative motion of the rotor blades. The trim was not done in order to obey the so called Modane law (Xb, Zb, β_S=0, β_C=-θ_S) but in order to meet the forces and moments.

Figure 14 shows the convergence of the control angles (θ_0, θ_S, θ_C) and the shaft angle α_q for the coupled 7A computations. The corresponding experimental values are given as square symbols. The computations were accepted as converged when the changes of the control angles and the shaft angle between two consecutive iterations were below 0.04°. The computation needed 5 iterations to converge.

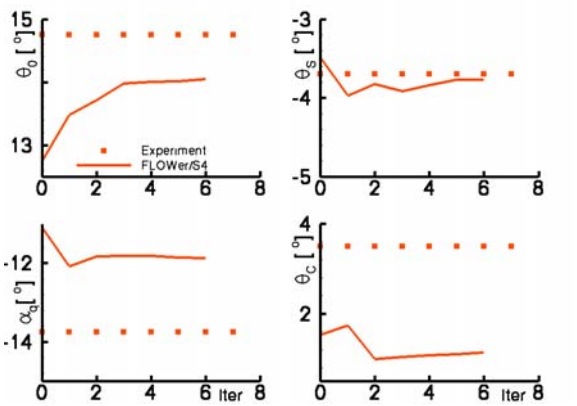

Figure 14 Convergence of control angles and shaft angle (7A rotor)

The largest differences between the computed control angles/shaft angle and the measured ones of more than 2° are observed for the control angle θ_C. The shaft angle and the other control angles show differences of 0.1° up to 2.0°, which is only a fair agreement. But it should be kept in mind that the CFD simulation was done assuming an isolated rotor in perfect free flight whereas the experimental setup includes the wind tunnel walls, the model support, the rotor hub etc.

A comparison of the normal force and the pitching moment distributions for the first (dotted line) and the fifth coupling iteration (solid line) with the experimental data is presented in Figure 15. Additionally the results of an isolated blade computation with the blade motion of the first trim was carried out (dash-dotted line). The effect of the wake system is obvious when comparing the results at r/R=0.825 of the isolated blade and the multi-bladed computation (dotted line) for trim 1.

On the first sight one may think that the coupling procedure does not improve the results compared to trim 1. But it should be kept in mind that the coupling procedure provides a trimmed solution *and* a fluid-structure coupling. The rotor is obviously not trimmed after trim 1 because the computed normal forces are below the measured ones for the whole rotor revolution at all three sections in Figure 15. When the solution is trimmed the overall agreement of the normal forces is considerably improved (Figure 15). Figure 16 compares the uncoupled S4 with the coupled FLOWer/S4 results and with the experimental data. There is an important improvement of the normal forces distribution in comparison with the experimental data because of the coupling with the 3D CFD method.

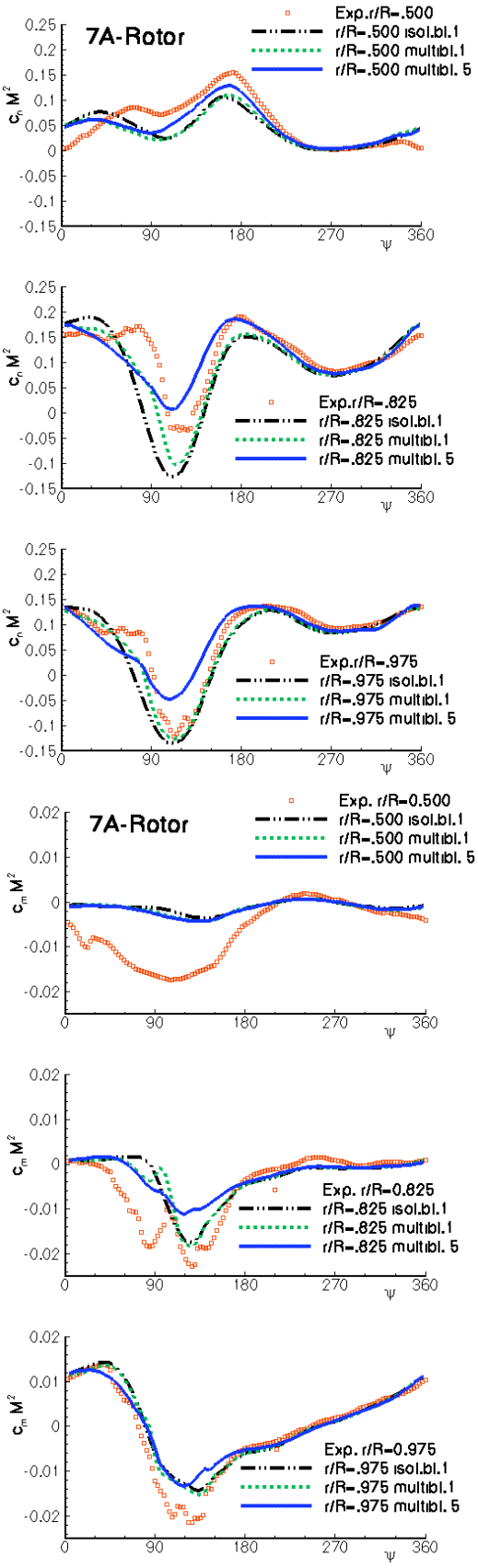

Figure 15 Normal forces and pitching moments distributions for the coupled FLOWer/S4 computations (7A rotor)

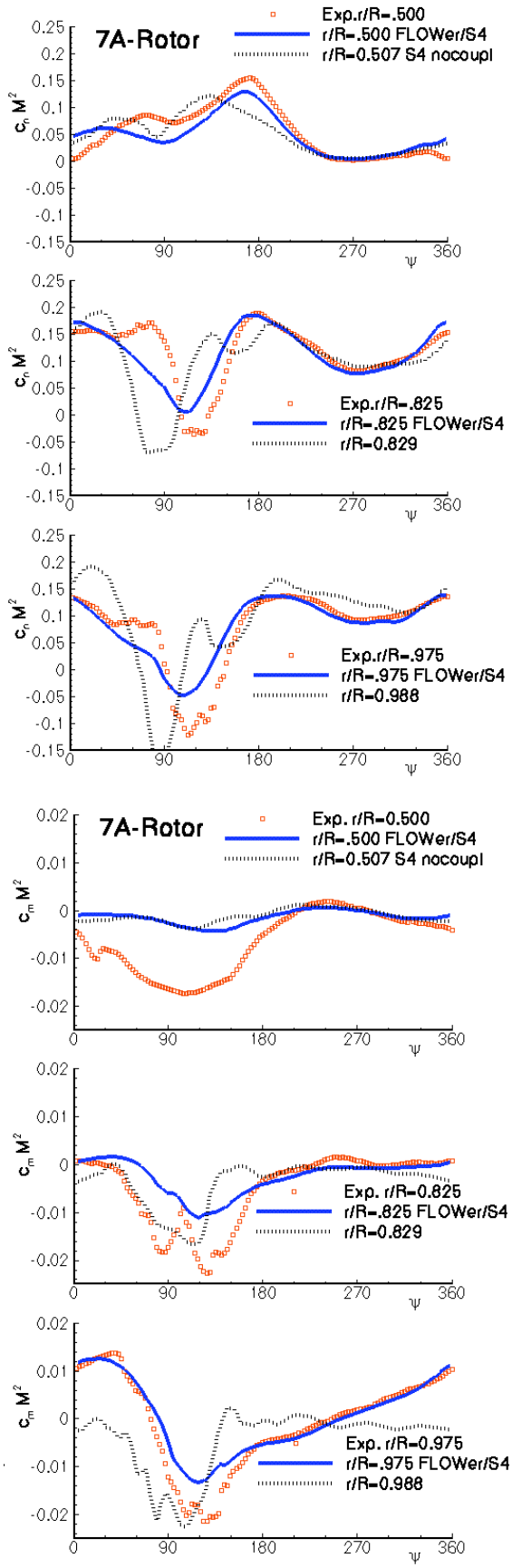

Figure 16 Normal forces and pitching moments distributions for the coupled FLOWer/S4 computations (7A rotor)

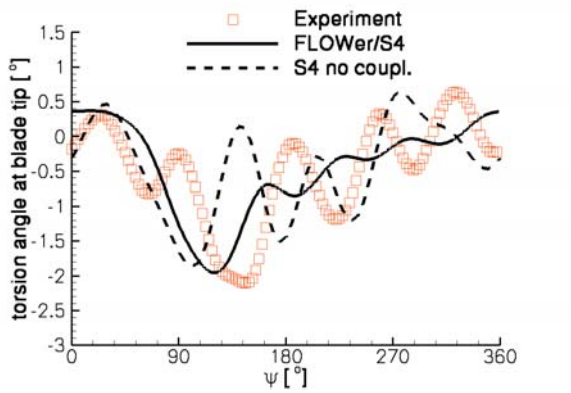

Figure 17 Elastic torsion at the blade tip (7A rotor)

Even a comprehensive rotor simulation code like S4 with a specific unsteady aerodynamic modelling is not capable to match the phase of the experimental data (see also [6]). The coupled results match qualitatively and quantitatively quite well although there is still a need for improvements.

The predicted elastic torsion at the blade tip of the uncoupled S4 computation and the coupled FLOWer/S4 computation is compared with the experimental results in Figure 17. The maximum elastic torsion at the blade tip is well captured by both computations. The phase of the maximum torsion deformation is slightly improved in the case of the coupling with FLOWer. The 5/rev content which is seen in the experimental data is reproduced by the S4 computation but it is almost completely damped out by the FLOWer/S4 computation. Since it was shown in [19] that a FLOWer/S4 coupling for a test case with a higher propulsive force is able to reproduce the 5/rev content it is assumed that the missing of the 5/rev content is not a systematic problem of the method. One possible explanation for the differences between the FLOWer/S4 predictions and the measurements is the assumption of an isolated rotor in a free stream within the CFD computations which does not seem to be appropriate when faced to the experimental setup, Figure 2, with wind tunnel walls, model support and rotor hub. The model support for example acts in fact like a kind of fuselage and produces upward induced velocities for ψ=180° and downward induced velocities for ψ=0°. The presence of the test rig inside the wind tunnel will modify the rotor trim considerably (see [24]).

Multi-bladed Computation for the 7AD Rotor with c_n+c_t+c_m-Coupling

In this chapter the results of multi-bladed computations for the 7AD rotor with c_n+c_t+c_m-coupling are presented and discussed.

The convergence of the control angles (θ_0, θ_S, θ_C) and the shaft angle α_q for the coupled 7AD computations is depicted in Figure 18. The corresponding experimental values are given as square symbols. The computations were accepted as converged when the changes of the control angles and the shaft angle between two consecutive iterations were below 0.04°. The computation needed 4 iterations to converge which is slightly faster than the computations for the 7A rotor. The lateral and the longitudinal control is in good agreement with the experimental data while the computed collective differs from the measured one by about half a degree and the difference in the shaft angle is about 2°. As in the 7A case the predicted absolute values of the shaft angle and the collective control angle are smaller than the corresponding experimental data.

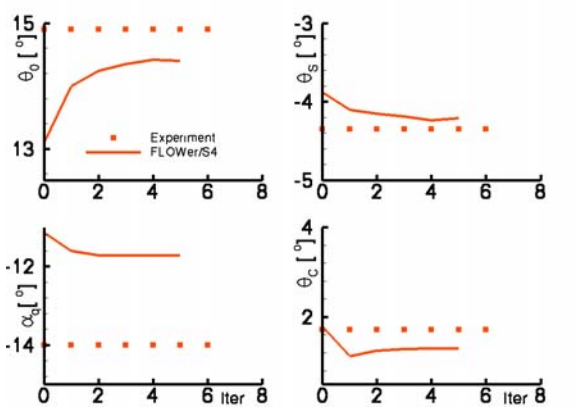

Figure 18 Convergence of control angles and shaft angle (7AD rotor)

Figure 19 shows the normal force distributions for r/R=0.7, 0.825 and 0.975. The section at r/R=0.7 was chosen as the most inboard section because no experimental data was available for this test case at r/R=0.5. The overall agreement after 4 coupling iterations between the predicted and measured normal forces in Figure 19 is only fair. The phase and the negative peak in the normal forces are only fairly reproduced by the simulation. The normal forces which were computed with the trim of the 0th coupling iteration compares extremely well at the blade tip with the wind tunnel measurements. But for all other sections the normal forces of trim 0 are below the measured values which means that the global thrust is too low. In order to meet the trim conditions the collective is considerably increased while the cyclic controls are reduced. This leads to a reduction in the negative peak in the normal forces and increases the differences between the predicted and measured normal forces at the blade tip.

A similar development during the coupling iterations is shown in Figure 20 for the pitching moment. For r/R=0.85 the CFD-results show a weak interaction of the rotor blade with the wake system at ψ=100°. This interaction disappears after 4 coupling iterations, which shows similar to the 7A test case that the flight conditions seen by the rotor in the wind tunnel differ qualitatively from those in the numerical simulation.

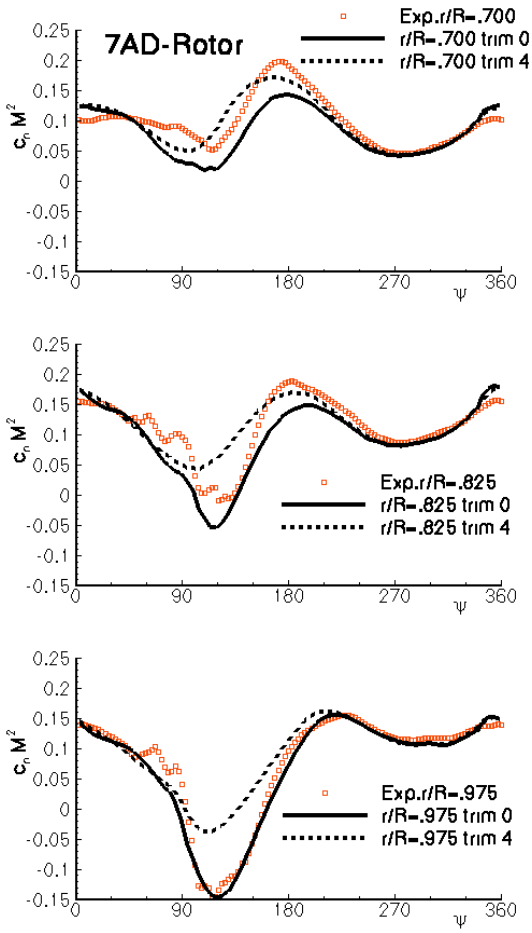

Figure 19 Normal force distributions for the coupled FLOWer/S4 computations (7AD rotor)

The elastic blade torsion is given in Figure 21. The blade torsion computed with the weak coupling of FLOWer and S4 does not show a 5/rev content whereas the uncoupled S4 computation does. The situation is similar as for the 7A case. The 5/rev content of the elastic torsion at the blade tip for the 7AD rotor is much smaller than for the 7A rotor. There are two reasons for this. One is the different aerodynamic behaviour of the two rotors. The 7AD rotor produces considerably lower pitching moments at the blade tip with a strong aerodynamic damping because of the planform which results in a lower excitation of 5 or 6/rev elastic torsion motions. Additionally the 7AD rotor has a torsional Eigenfrequency which is between 6 and 7/rev while the Eigenfrequency of the 7A rotor is almost exactly 6/rev. Therefore elastic oscillations are more easily excited in the case of the 7A rotor. This is in fact also the reason for the different convergence behaviour of the weakly coupled computations for the two rotors.

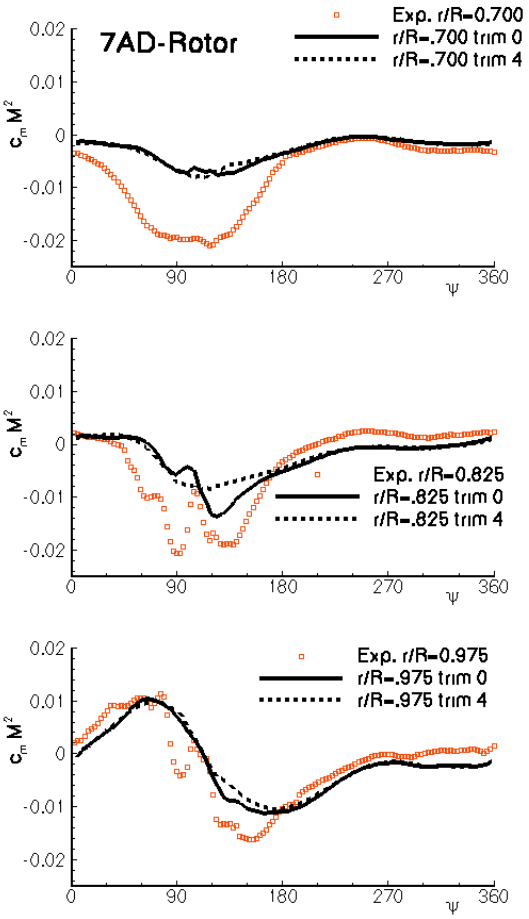

Figure 20 Pitching moment distributions for the coupled FLOWer/S4 computations (7AD rotor)

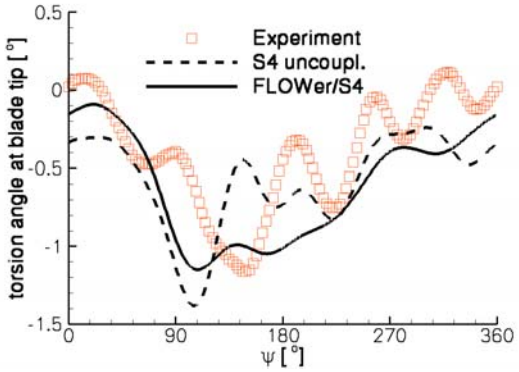

Figure 21 Elastic torsion at the blade tip (7AD)

Synthesis of 7A and 7AD results

The weak coupling with normal forces, tangential forces and pitching moments based on Navier-Stokes computations predicted the normal force distributions quite well. The predicted local pitching moments showed for both rotors considerable differences to the experimental data for r/R=0.5/0.7. The agreement of predicted and measured moments close to the blade tip was quite good.

Table 2: Computational Effort

Description	Rotor	CPU-Time [h]/Rev on 1 Proc. NEC-SX5
N-S chimera	7A	50
N-S chimera	7AD	55

The computational effort is given in Table 2. For this kind of application which includes deforming meshes and chimera functionalities a performance of only 1.0 GFLOPS is obtained on one processor of the DLR NEC-SX5. The reason for this poor performance is that part of the chimera search and most parts of the grid deformation tool in FLOWer 116.6 are not well vectorized.
The predicted and measured power consumption of the 7A and the 7AD rotor are presented in Figure 22. All power evaluations were done within the S4 code and the coupling with multi-bladed CFD computations was considered. The S4 code alone underpredicts the power consumption by 23.6% for the 7A and 21.2% for the 7AD rotor whereas the coupled computations overpredict the absolute power consumption by 9% for the 7A and 11% for the 7AD rotor. The predicted absolute power with the chimera approach is considerably closer to the wind tunnel measurements than the isolated blade results of [19]. The agreement between simulation and measurement for the absolute values is improved by the weak coupling and is satisfactory if one keeps in mind that fully turbulent computations were carried out. The effect of transition from laminar to turbulent boundary layer will reduce the rotor power by several percent (about 5% were obtained for the 7A rotor in hover in [25]). The blade stubs were not gridded for this investigation which produces a too strong vortex at the blade root. A reduction in power of about 4-5% when accounting for the blade stubs can be expected (see [26]). Still it may be assumed that the aforementioned effects will modify the predictions for the two rotors similarly. When the prediction of the power difference between the two rotors is compared a considerable improvement because of the weak coupling can be observed. With the weak coupling a reduction in power consumption when comparing the 7AD and the 7A rotor of about 3.5% is predicted which compares fairly well to the measured 5.5% reduction.

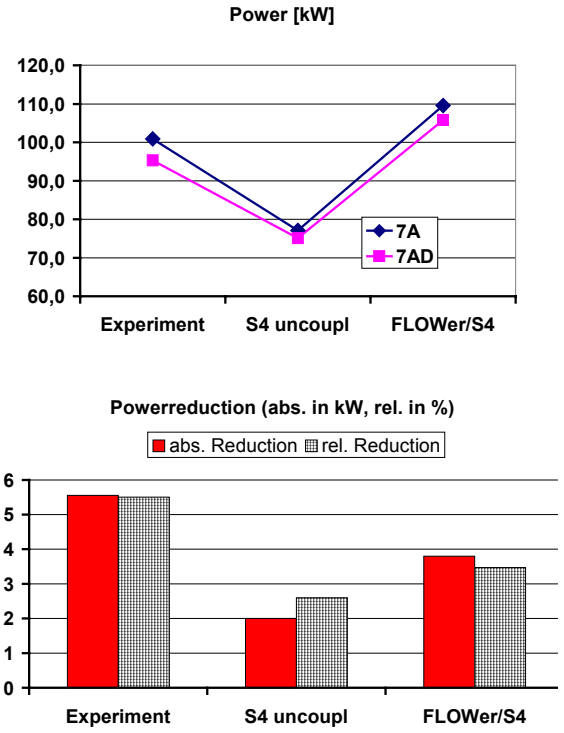

Figure 22 Power for 7A and 7AD rotor and power difference between these rotors

Conclusion

A weak coupling procedure for coupling the rotor simulation code S4 and the RANS solver FLOWer which exchanges the local normal forces, tangential forces and pitching moments was presented. The method allows to produce trimmed CFD solutions for rotors in high-speed forward flight accounting for elastic blade deformations and viscous effects. The weak coupling procedure was applied to high-speed forward flight test cases of the 7A and the 7AD rotor. Multi-bladed computations were carried out for both rotors.
It turned out that for this type of test cases of rotors in high-speed forward flight with moderate loading 2-equation turbulence models do not improve the prediction significantly compared to the Baldwin-Lomax turbulence model.
An overall improvement of the solution with respect to the existing experimental data because of the weak coupling was proven. The well known negative peak in the normal forces distribution close to the blade tip around 90°-

120° for elastic blades in high-speed forward flight was reproduced with the coupled Navier-Stokes computations. Even the phase agrees fairly well. There was a considerable difference in control settings, which means that the flight condition seen by the CFD simulation is not the same as in the wind tunnel. One possible explanation may be the interference effects between the rotor, the wind tunnel walls, the model support and the rotor hub which where not present in CFD grid system which contained only an isolated rotor. The Chimera method is able to predict the weak interaction of the rotor blades with the vortex-system although the final converged state showed almost no blade-vortex interaction. The 5/rev content in the 7A blade tip torsion was damped out in the coupled computations because the final trim showed strongly reduced peaks in c_n and c_m.
The performance differences between the 7A and the 7AD rotor in high-speed forward flight was well predicted although the absolute power was overpredicted for both rotors by about 10%.

For an industrial application the user workload has to be considerably reduced by automatisation of the coupling procedure. Furthermore a significant reduction of the computational effort is required.

References

[1] Tung, C., Caradonna, F.X., Johnson, W.: "The Prediction of Transonic Flow on an Advancing Rotor", Journal of the American Helicopter Society, Vol. 31, No 3, July 1986, pp 4-9.

[2] Servera, G.; Beaumier, Ph.; Costes, M.: "A weak coupling method between the Dynamics code HOST and the 3D Unsteady Euler code WAVES", 26th ERF Forum, Sept. 2000.

[3] Pahlke, K.; Van der Wall, B. G.: "Calculation of Multibladed Rotors in High-Speed Forward Flight with weak Fluid-Structure-Coupling", 27th European Rotorcraft Forum, Moscow, Sept.11-14, 2001.

[4] Altmikus, A. R. M.; Wagner, S.; Beaumier, P. and Servera, G.: "A Comparison: Weak vs Strong Modular Coupling for Trimmed Aeroelastic Rotor Simulations", 58th AHS Forum, Montreal, Canada, June 11-13, 2002.

[5] Sitaraman, J.; Baeder, J.D. and Chopra, I.: "Validation of UH-60 Rotor Blade Aerodynamic Characteristics using CFD", 59th AHS Forum, Phoenix, Arizona, May 6-8, 2003.

[6] Sitaraman, J.; Datta, A.; Baeder, J.D. and Chopra, I.: "Fundamental Understanding and Prediction of Rotor Vibratory Loads in High-Speed Forward Flight", 29th ERF Forum, Friedrichshafen, Germany, Sep. 16-18, 2003.

[7] Kroll, N.; Rossow, C.C.; Becker, K. and Thiele, F.: "MEGAFLOW-A Numerical Flow Simulation system", ICAS-congress, September 1998, Melbourne, Australia.

[8] Pahlke,K.: "Berechnung von Strömungsfeldern um Hubschrauberrotoren im Vorwärtsflug durch die Lösung der Euler-Gleichungen", DLR-Forschungsbericht 1999-22, ISSN 1434-8454, 1999.

[9] Jameson, A.; Schmidt, W. and Turkel, E.: "Numerical Solutions of the Euler Equations by Finite Volume Methods Using Runge-Kutta Time-Stepping Schemes", AIAA Paper 81-1259, 1981

[10] Baldwin, B. and Lomax, H., "Thin Layer Approximation and Algebraic Model For Separated Turbulent Flows", AIAA-Paper 78-0257,197

[11] Degani and Schiff, L., "Computation of Turbulent Supersonic Flows around Pointed Bodies having Crossflow Separation", Journal of Computational Physics Vol. 66, pp. 176-196, 1986.

[12] Wilcox, D. C., "Reassessment of the Scale-Determining Equation for Advanced Turbulence Models", AIAA-Journal, Vol. 26, pp. 1299-1310, 1988.

[13] Rung, T. et. al., "Assessment of Explicit Algebraic Stress Models in Transonic Flows", Proc. 4th Int. Symposium on Engineering Turbulence Modelling and Measurements, Corsica, France, 1999, pp. 659-668.

[14] Dol, H. S.; Kok, J. C. and Oskam, B.: "Turbulence Modelling for Leading-Edge Vortex Flows", AIAA 2002-0843.

[15] Jameson, A.: "Time Dependent Calculation Using Multigrid, with Applications to Unsteady Flows Past Airfoils and Wings", AIAA Paper 91-1596, 1991.

[16] Gaitonde, A. L. and Fiddes, S.: "A Three-Dimensional Moving Mesh Method for the Calculation of Unsteady Transonic Flows", University of Bristol, Rep. No. 483, Sept. 1993.

[17] van der Wall, B. G.: "An Analytical Model of Unsteady Profile Aerodynamics and its Application to a Rotor Simulation Program", 15th European Rotorcraft Forum, Amsterdam, Netherlands, 1989.

[18] van der Wall, B. G.: "Analytic Formulation of Unsteady Profile Aerodynamics and its Application to Simulation of Rotors", DLR-FB 90-28, 1990, also: ESA-Report No. ESA-TT-1244, 1992.

[19] Pahlke, K. and van der Wall, B. G.: "Progress in Weak Fluid-Structure-Coupling for Multibladed Rotors in High-Speed Forward Flight, 28th European Rotorcraft Forum, Paper 67, Bristol, UK, 2002.

[20] Beaumier, P.; Prieur, J.; Rahier, G.; Spiegel, P.; Demargne, A.; Tung, C.; Gallmann, J.M.; Yu, Y.; Kube, R.; van der Wall, B. G.; Schultz, K.J.; Splettstoesser, W.R.; Brooks, T.F.; Burley, C.L.; Boyd, D.D.: "Effect of Higher Harmonic Control on Helicopter Rotor Blade-Vortex Interaction Noise: Prediction and Initial Validation", AGARD-CP-552, 1995; also: 75th Fluid Dynamics Symposium, Berlin, Germany, 1994

[21] Petot, D.; Arnaud, G.; Harrison, R.; Stevens, J.; Teves, D.; van der Wall, B. G.; Young, C. and Széchényi, E.: "Stall Effects and Blade Torsion -

an Evaluation of Predictive Tools", 23rd European Rotorcraft Forum, Dresden, Germany, 1997.

[22] Allongue, M. and Drevet, J.P.: “New Rotor Test Rig in the Large Modane Wind Tunnel”, 15th ERF, September 12-15, 1989, Amsterdam.

[23] Beaumier, P.; Costes, M. and Gavériaux, R.: "Comparison Between FP3D full Potential Calculations and S1 Modane Wind Tunnel Test Results on Advanced Fully Instrumented Rotors" 19th ERF, Cernobbio, Como (Italy), Sept. 1993.

[24] Masson, A. and Beaumier, P.: “Prise en Compte des Effets de Paroi de la Soufflerie S1MA dans les Calculs de Mise en Equilibre du Rotor”, ONERA RTS 12/3732 AY, 1993.

[25] Beaumier, P.; Chelli, E. and Pahlke, K. “Navier-Stokes Prediction of Helicopter Rotor Performance in Hover Including Aero-Elastic Effects”, 56th AHS Forum, May 2-4, 2000.

[26] Beaumier, P.; Brezillon, J.: “Numerical Investigation on the Influence of Blade Roots (Stubs) on Hovering Rotors”, 27th European Rotorcraft Forum, Moscow, Russia, 2001.